Tran-SET

Transportation Consortium of South-Central States

*Solving Emerging Transportation Resiliency, Sustainability, and Economic Challenges through the Use of Innovative Materials and Construction Methods: From Research to Implementation*

# Calculating Pile Downdrag: Experimental and Numerical Investigations

**Project No. 20GTLSU10**

**Lead University: Louisiana State University**

**Final Report**

**October 2021**

**Disclaimer**

The contents of this report reflect the views of the authors, who are responsible for the facts and the accuracy of the information presented herein. This document is disseminated in the interest of information exchange. The report is funded, partially or entirely, by a grant from the U.S. Department of Transportation's University Transportation Centers Program. However, the U.S. Government assumes no liability for the contents or use thereof.

**Acknowledgements**

The authors acknowledge the financial support for this study by the Transportation Consortium of South Central States (Tran-SET).

# TECHNICAL DOCUMENTATION PAGE

| | | |
|---|---|---|
| **1. Project No.**<br>20GTLSU10 | **2. Government Accession No.** | **3. Recipient's Catalog No.** |
| **4. Title and Subtitle**<br><br>Calculating Pile Downdrag: Experimental and Numerical Investigations | | **5. Report Date**<br>Oct. 2021<br>**6. Performing Organization Code** |
| **7. Author(s)**<br>PI: Hai Lin https://orcid.org/0000-0002-1641-4588<br>Co-PI: Shengli Chen http://orcid.org/0000-0002-5595-8692<br>GRA: Hussein Alqrinawi https://orcid.org/0000-0001-5972-9339 | | **8. Performing Organization Report No.** |
| **9. Performing Organization Name and Address**<br>Transportation Consortium of South-Central States (Tran-SET)<br>University Transportation Center for Region 6<br>3319 Patrick F. Taylor Hall, Louisiana State University, Baton Rouge, LA 70803 | | **10. Work Unit No. (TRAIS)**<br><br>**11. Contract or Grant No.**<br>69A3551747106 |
| **12. Sponsoring Agency Name and Address**<br>United States of America<br>Department of Transportation<br>Research and Innovative Technology Administration | | **13. Type of Report and Period Covered**<br>Final Research Report<br>Aug. 2020 – Aug. 2021<br>**14. Sponsoring Agency Code** |
| **15. Supplementary Notes**<br>Report uploaded and accessible at Tran-SET's website (http://transet.lsu.edu/). | | |


**16. Abstract**

Piles can be exposed to significant settlement (i.e., downdrag) and compressive force (i.e., dragload) if embedded in consolidating ground. Downdrag has been included in the design of piles, but there is uncertainty about how downdrag and dragload are efficiently considered in the pile design due to the differences in the existing design methods (e.g., AASHTO and FHWA). Although several field monitoring programs were successfully conducted on pile downdrag, fully instrumented pile model tests are still needed to investigate the responses at the soil-pile interface to improve the design of pile downdrag. This research focused on investigating the downdrag and skin friction at the soil-pile interface using fully instrumented small-scale pile tests. An aluminum pile (51×102×508 mm) was subjected to downdrag in a consolidating loose sand deposit. Innovative interface shear stress sensor ($S_3F$) and strain gauges were installed on the pile surface to measure the drag forces and skin frictions at the soil-pile interface. Settlement plates were installed in the soil at different locations to measure the soil settlement profile. The $S_3F$ sensor was calibrated in the lab. Position transducers were also attached to the head and tip of the pile to measure the pile settlement profile. The lab test results will be used to calibrate a numerical model that can predict pile downdrag with a high level of accuracy, which can provide a more realistic estimation of pile downdrag, avoid the conservative pile foundation design, and possibly reduce the foundation cost.


| | | | |
|---|---|---|---|
| **17. Key Words**<br>Soil-Pile Interaction, Downdrag, Drag Load, Lab-Scale Tests | **18. Distribution Statement**<br>No restrictions. This document is available through the National Technical Information Service, Springfield, VA 22161. | | |
| **19. Security Classif. (of this report)**<br>Unclassified | **20. Security Classif. (of this page)**<br>Unclassified | **21. No. of Pages**<br>29 | **22. Price** |

**Form DOT F 1700.7 (8-72)** **Reproduction of completed page authorized.**

# SI* (MODERN METRIC) CONVERSION FACTORS

## APPROXIMATE CONVERSIONS TO SI UNITS

| Symbol | When You Know | Multiply By | To Find | Symbol |
|---|---|---|---|---|
| | | **LENGTH** | | |
| in | inches | 25.4 | millimeters | mm |
| ft | feet | 0.305 | meters | m |
| yd | yards | 0.914 | meters | m |
| mi | miles | 1.61 | kilometers | km |
| | | **AREA** | | |
| $in^2$ | square inches | 645.2 | square millimeters | $mm^2$ |
| $ft^2$ | square feet | 0.093 | square meters | $m^2$ |
| $yd^2$ | square yard | 0.836 | square meters | $m^2$ |
| ac | acres | 0.405 | hectares | ha |
| $mi^2$ | square miles | 2.59 | square kilometers | $km^2$ |
| | | **VOLUME** | | |
| fl oz | fluid ounces | 29.57 | milliliters | mL |
| gal | gallons | 3.785 | liters | L |
| $ft^3$ | cubic feet | 0.028 | cubic meters | $m^3$ |
| $yd^3$ | cubic yards | 0.765 | cubic meters | $m^3$ |
| | | NOTE: volumes greater than 1000 L shall be shown in $m^3$ | | |
| | | **MASS** | | |
| oz | ounces | 28.35 | grams | g |
| lb | pounds | 0.454 | kilograms | kg |
| T | short tons (2000 lb) | 0.907 | megagrams (or "metric ton") | Mg (or "t") |
| | | **TEMPERATURE (exact degrees)** | | |
| $^oF$ | Fahrenheit | 5 (F-32)/9<br>or (F-32)/1.8 | Celsius | $^oC$ |
| | | **ILLUMINATION** | | |
| fc | foot-candles | 10.76 | lux | lx |
| fl | foot-Lamberts | 3.426 | candela/$m^2$ | $cd/m^2$ |
| | | **FORCE and PRESSURE or STRESS** | | |
| lbf | poundforce | 4.45 | newtons | N |
| $lbf/in^2$ | poundforce per square inch | 6.89 | kilopascals | kPa |

## APPROXIMATE CONVERSIONS FROM SI UNITS

| Symbol | When You Know | Multiply By | To Find | Symbol |
|---|---|---|---|---|
| | | **LENGTH** | | |
| mm | millimeters | 0.039 | inches | in |
| m | meters | 3.28 | feet | ft |
| m | meters | 1.09 | yards | yd |
| km | kilometers | 0.621 | miles | mi |
| | | **AREA** | | |
| $mm^2$ | square millimeters | 0.0016 | square inches | $in^2$ |
| $m^2$ | square meters | 10.764 | square feet | $ft^2$ |
| $m^2$ | square meters | 1.195 | square yards | $yd^2$ |
| ha | hectares | 2.47 | acres | ac |
| $km^2$ | square kilometers | 0.386 | square miles | $mi^2$ |
| | | **VOLUME** | | |
| mL | milliliters | 0.034 | fluid ounces | fl oz |
| L | liters | 0.264 | gallons | gal |
| $m^3$ | cubic meters | 35.314 | cubic feet | $ft^3$ |
| $m^3$ | cubic meters | 1.307 | cubic yards | $yd^3$ |
| | | **MASS** | | |
| g | grams | 0.035 | ounces | oz |
| kg | kilograms | 2.202 | pounds | lb |
| Mg (or "t") | megagrams (or "metric ton") | 1.103 | short tons (2000 lb) | T |
| | | **TEMPERATURE (exact degrees)** | | |
| $^oC$ | Celsius | 1.8C+32 | Fahrenheit | $^oF$ |
| | | **ILLUMINATION** | | |
| lx | lux | 0.0929 | foot-candles | fc |
| $cd/m^2$ | candela/$m^2$ | 0.2919 | foot-Lamberts | fl |
| | | **FORCE and PRESSURE or STRESS** | | |
| N | newtons | 0.225 | poundforce | lbf |
| kPa | kilopascals | 0.145 | poundforce per square inch | $lbf/in^2$ |

# TABLE OF CONTENTS

## LIST OF FIGURES

## ACRONYMS, ABBREVIATIONS, AND SYMBOLS

| | |
|---|---|
| AASHTO | American Association of State Highway & Transportation. Officials |
| DOTs | Departments of Transportation |
| FHWA | Federal Highway Administration |
| $f_s$ | Skin Friction |
| $k$ | Lateral Earth Pressure Coefficient |
| LVDTs | Linear Variable Displacement Transducers |
| $S_3F$ | Surface Stress Sensitive Film Sensor |
| $\tan\delta$ | Interface Friction Angle |
| $\sigma_z'$ | Vertical Effective Stress |

## EXECUTIVE SUMMARY

The goal of this research is to investigate pile downdrag in consolidating ground using lab-scale pile tests instrumented with Surface Stress Sensitive Film ($S_3F$) sensor, strain gauges, and settlement plates. The test results will be used to calibrate a numerical modeling tool that can accurately predict downdrag and drag load along the pile. The project consisted of five primary research tasks. The first task involves an in-depth literature review of previous studies related to pile downdrag analysis to fully understand the pile behavior subjected to downdrag and provide references for planning lab-scale pile tests. Second task involves the calibration of the advanced $S_3F$ sensor under similar conditions at the pile-soil interface. $S_3F$ sensors can measure soil-pile interface negative and positive skin frictions and normal pressure over the sensor surface. Using such innovative sensor at the pile-soil interface promises accurate measurement of drag load and lateral earth pressure coefficient ($k$) at the soil-pile interface. The third task involves a series of lab-scale instrumented pile tests to measure the drag load, downdrag, and neutral plane along the pile length. This phase included floating pile and end bearing pile tests. The interface direct shear tests (task four) were also performed to investigate the interface shear behavior between the soil and pile. The final task involves the development of a comprehensive numerical model using ABAQUS finite element package to investigate the downdrag and drag load mobilized at the pile-soil surface as well as the overall settlement responses of the pile with time. The ABAQUS model will be first compared with the experimental test data obtained from the previous research tasks, which will then be adopted to conduct extensive parametric analyses to cover various combinations of pile properties and soil conditions existing in Louisiana.

# 1. INTRODUCTION

The axial resistance of deep foundations can be divided into two components: shaft resistance and tip resistance. The direction of the shaft resistance depends on the relative movement between the deep foundation and the adjacent soil. If the pile moves downward relative to the soil, the positive shaft resistance is developed (i.e., shaft resistance acting upward). Conversely, If the soil moves downward relative to the pile, the negative shaft resistance is developed (i.e., shaft resistance acting downward). The drag load is defined as the axial compressive load induced along the length of the pile due to the accumulated negative skin friction. Downdrag is defined as the downward movement of a pile that results from the ground settlement. The neutral plane is at the location where the negative shear changes to the positive shear direction.

Pile foundations embedded in consolidating soil profiles (i.e., soil experiencing settlement due to surcharge loading, groundwater level drop, liquefaction, etc.) are subjected to increased axial loads (i.e., drag load) and pile settlements (i.e., downdrag). Downdrag has been reported to have caused extreme foundation movements, differential settlements, and extensive damage to various structures in south-central states. Downdrag has long been included in the design of transportation foundations subjected to ground settlement, and it is ubiquitous in Region 6 states. There are currently inconsistencies in how downdrag and drag load are incorporated into the pile design, partly due to the differences of design methods in the design codes (e.g., AASHTO LRFD Bridge Design Specifications and FHWA Driven Pile Manual). State DOTs are facing a design challenge about the inconsistencies of design codes (i.e., AASHTO LRFD Bridge Design Specifications and FHWA Driven Pile Manual) to predict drag load and downdrag. A preliminary analysis of a hypothetical pile showed that pile design could be significantly more conservative and costlier when using AASHTO LRFD Bridge Design Specifications. Therefore, there is an immediate need to investigate the fundamental behavior of piles subject to downdrag for updating the design specifications. Although several field monitoring programs in the literature were successfully conducted on piles under downdrag, fully instrumented lab-scale pile tests focusing on the responses at the soil-pile interface is still lacking, which was investigated in this project. Furthermore, Dr. Fellenius developed the neutral plane method and reported that the soil settlement and the pile settlement are identical at the neutral plane. However, the neutral plane definition in this method may deviate from the actual loading conditions. For example, soil effective stress increases during soil consolidation, thereby resulting in time-varying neutral plane locations.

This research focuses on investigating the soil-pile interaction during pile downdrag. S3F interface shear stress sensor, strain gauges, and settlement plates were used to measure downdrag, drag load, and location of neutral plane. The test results of this research will update the current design specifications of downdrag calculation. This research will also develop a ready-to-use numerical modeling tool.

## 2. OBJECTIVES

The main objective of this study is to investigate pile downdrag in consolidating ground using fully instrumented lab-scale pile tests. To accomplish the proposed objective, the following tasks were conducted:

Task 1 involved a systematic review of literature on pile downdrag. The literature review was used to (1) collect experimental studies to fully understand the pile behavior subjected to downdrag and provide references for planning lab-scale pile tests; and (2) investigate available modeling methods of pile downdrag and provide guidance for future finite element analysis for the lab-scale pile tests.

Task 2 consisted of performing the calibration of $S_3F$ interface shear stress sensor under similar conditions at the pile-soil interface. $S_3F$ sensors can measure soil-pile interface negative and positive skin frictions and normal pressure over the sensor surface. Using such innovative sensor at the pile-soil interface promises accurate measurement of the shaft resistance at the soil-pile interface. The effect of the loading area on the calibration relationship was investigated. The effects of the soil particle size, saturation condition, and temperature will also be investigated.

Task 3 encompassed series of lab-scale instrumented pile tests to measure the drag load, downdrag, and neutral plane along the pile length. Two pile tests were accomplished to investigate pile behavior under different soil relative densities and pile conditions, including a floating pile in sand deposits with relative densities of ~30% (test No. 1) and an end-bearing pile in sand deposits with relative densities of ~30% (test No. 2). This task will also predict pile downdrag, drag load, and neutral plane locations using different design methods (e.g., AASHTO LRFD Bridge Design Specifications, FHWA Driven Pile Manual, and Fellenius' unified design approach). The predicted data will be used to compare to the lab-scale test results. This comparison will help assess those design methods and help improve the design specifications.

Task 4 investigated the interface shear behavior between the soil and pile using direct shear tests. The direct shear test setup was modified to use the pile material (i.e., aluminum) as the bottom shear box. Ottawa 50-70 sand was prepared in the upper shear box. The responses at the soil-pile interface under various overburden pressures (e.g., 15, 35, 50, 70, 100, 125, 150, 175 kPa) were investigated.

Task 5 included the development of a comprehensive numerical model, using ABAQUS finite element package, to investigate the downdrag and drag load mobilized at the pile-soil surface as well as the overall settlement responses of the pile with time. The ABAQUS computations will first be compared with the experimental test data obtained from the previous phase, and once fine-tuned/calibrated, will be adopted to conduct extensive parametric analyses to cover various combinations of the pile properties and soil conditions, especially those in close relevance to the conditions encountered in the state of Louisiana.

## 3. LITERATURE REVIEW

Downdrag has been reported to cause extreme foundation movements, differential settlements, and extensive damage to various structures. For example, Inoue et al *(1)* reported a case history for a three-story building located in the south west corner of Edogawa delta facing the Tokyo Bay. Despite the pile foundations of the building had a sufficient geotechnical capacity to sustain the applied loads from the building, noticeable amount of settlement had been observed. The investigation in this case attributed that there was around 20 cm of additional settlement. This additional settlement was due to the pumping of water out of a soil layer located beneath the neutral plane of the piles. As a result, the building was not able to serve any more and had to be demolished.

Ignoring pile downdrag may result in serviceability problems caused by downdrag and structural failure caused by drag load *(2).* There are several remediation methods for reducing the downdrag and drag load: (1) using a preloading method to reduce soil settlement before pile installation; (2) using casing to prevent direct contact between the pile and soil; and (3) reducing negative skin friction by applying a coating (e.g., Teflon and bitumen) around the pile. However, the effectiveness of the coating method should be evaluated under different temperatures and loading conditions *(3).* For example, Budge et al. *(4)* performed several field monitoring tests of driven piles with and without Teflon coating in Minnesota. They reported that the effectiveness of the Teflon coating in reducing drag load was limited. Fellenius *(5)* also stressed that although the bitumen coating could reduce the negative skin friction, drag load, and possibly downdrag. However, the bitumen coating will also reduce the geotechnical capacity and the factor of safety of the pile in carrying the applied load.

Chow and Wong *(6)* studied the efficiency of low-density polyethylene sheets (LDPE) on reducing the drag forces on the deep foundations. In this study, the effect of the number of LDPE layers was investigated. It was observed that using two or three layers of LDPE could mitigate the skin friction by around 90% with slight difference in their efficiency. Chow and Wong *(6)* also reported that the LDPE layers remained as a unit and no distortion was found. Lam et. al *(2)* investigated the efficiency of sacrificial sleeves to minimize the negative skin friction (drag load) on deep foundations. This method was found to be effective in reducing the drag load and downdrag because of the interaction between the consolidating ground and the sleeve instead of the interaction between the soil and the pile itself. Lam et. al *(2)* also compared the sacrificial sleeves method and the group of sacrificial piles method on reducing the drag forces on the deep foundations by conducting centrifuge tests and numerical simulations. The study found that the sacrificial sleeves were more efficient in the skin friction reduction as compared to the sacrificial piles. It was also reported that the sacrificial sleeves method could be cheaper, more environmentally friendly, and easy to apply as compared to other methods. The main factor, which was found to mostly affect the efficiency of the shielding, was the length of the sacrificial sleeves *(2).*

Walker et al. *(7)* investigated the efficiency of the bitumen coated piles as compared to the uncoated piles. In their study, they drove bitumen-coated pipe pile and uncoated one in a consolidating ground. A fill layer was placed over the area of the piles to consolidate the ground. After soil settlement, significant large drag forces were induced along the uncoated pile length. On the other hand, insignificant negative skin friction was developed along the bitumen-coated pile during the soil settlement. However, the soil settlement at the surface ground level was small

during the observation period. It was also noted that the pile downdrag was not significant because most of the pile head settlement was due to the elastic shortening of the pile as a result of the applied loads *(7)*.

Tawfiq *(8)* studied the efficiency of the polyethylene sheets in reducing the drag forces on the deep foundations. In this study, the effects of the temperature and the rate of soil displacement were investigated, and a comparison between the polyethylene sheets and the bitumen coating was accomplished. It was observed that the reduction of the bitumen viscosity under relatively high temperature could increase the shaft resistance. That was due to the complete permeation of the soil particles through the bitumen layer, which eventually caused a significant increase in the shaft resistance. It was also noticed that several factors should be taken into consideration for bitumen coated deep foundations such as particle sizes, surrounding temperature, and rate of soil displacement. On the other hand, the skin friction of the piles with a polyethylene sheeting showed independency from particle sizes, surrounding temperature, and rate of soil displacement, with an efficiency reached around 78%.

The efficiency of downdrag reducing method should be evaluated as a whole combination including pile material, friction reducing procedure, and soil types. The evaluation should also be conducted under different circumstances and loading conditions. It is important to note that the effectiveness of the Teflon coating in reducing drag load was limited. Fellenius *(5)* also stressed that although the bitumen coating could reduce the negative skin friction, drag load, and possibly downdrag. However, the bitumen coating will also reduce the geotechnical capacity and the factor of safety of the pile in carrying the applied load.

Fellenius *(9)* reported that the pile performance under downdrag depends on its location within the group of piles. It was also found that the inner piles within a group of piles has a minimal drag forces and the positive side resistance develops close from the tip of the pile foundation *(9)*. However, the perimeter piles will experience drag forces and additional pile settlement if embedded inside a subsiding soil. The difference in the performance of the perimeter and interior piles is because the interior piles transfer their loads to the surrounding soil starting from the tip of the pile. On the other hand, the perimeter piles behave in the same way as the single piles.

Fellenius *(10)* investigated pile drag load and downdrag using several full-scale long-term pile tests data and proposed a unified design approach to calculate the drag load and downdrag. Based on the analysis of several long-term pile tests, Fellenius *(5)* concluded that the interface skin friction was governed by the effective stress and the ultimate skin friction could be mobilized by a tiny movement. The drag load and downdrag are inter-related since the downdrag determines the amount of pile toe penetration into the soil, which will determine the pile toe resistance and affect the location of the neutral plane.

The amplitude of pile downdrag is equal to the corresponding soil settlement at the neutral plane, as shown in Figure 1. Siegel et al. *(11)* examined the current AASHTO specifications and presented an alternative design approach for calculating drag load and downdrag using Fellenius' unified design approach. Siegel et al. *(11)* recommended that the drag load should not be included in the load combinations when considering the geotechnical strength limit state. The drag load should be estimated using Fellenius' unified design approach and should not be included in the top load combinations for settlement analysis. Furthermore, the pile downdrag should be equal to the soil settlement at the neutral plane.

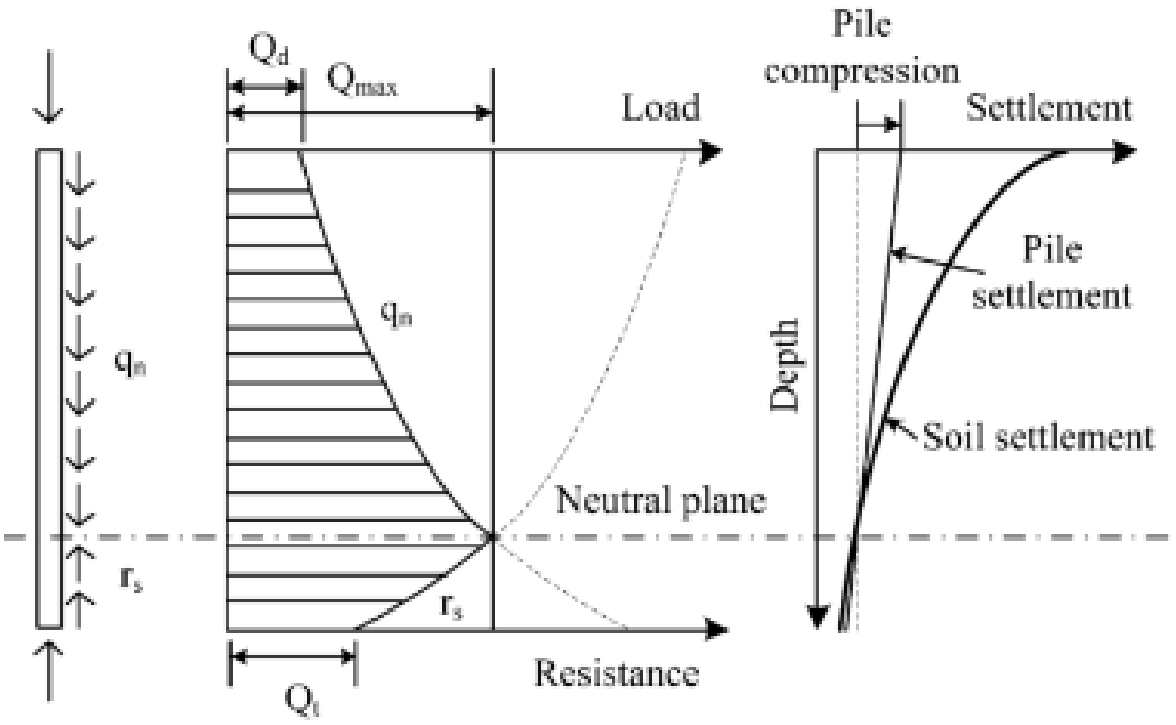


**Figure 1. Illustration of the unified design approach *(9)*.**

Sears *(12)* investigated the performance of steel piles driven in consolidating ground. In this study, the field tests measured the accumulation of negative skin friction before and after the construction of the bridge. The first case represented by applying the construction loads before ending the consolidation process. Decreasing in drag forces was observed immediately after applying the structural loads prior to the fill placement. However, the load above the neutral plane continuously increased because of the soil settlement after the fill placement. The load above the neutral plan stopped the increasing when the original load at the neutral plan increased by the same value of the applied load on the top of the pile *(12)*. The second case represented by applying the construction loads after the ending of consolidation process. Positive skin friction was also developed from the top of the pile downward, but the increase in the load at the neutral plan was not more than the half of the applied load at the top of the pile *(12)*.

Obake *(13)* observed the redevelopment of the negative skin friction along the pile length after the drag load decrease due to the construction load applied on the pile. In this study, long pipe piles of 43m were driven in a consolidating ground and the soil was consolidated by applying a fill placement over the area of the pile and pumping out the water to lower the pore pressure. For the case of monitoring the drag load before applying the construction load, the drag forces along the pile increased continuously with soil settlement. It was also found that the location of the neutral plane was around 40 m below the top of the pile. However, after applying a load of 700 kN on the pile head, the negative skin friction reduced accordingly for a short period of time. After that, a redevelopment of the negative skin friction was noted with a reduction in the depth of the neutral plane by 10 m *(13)*.

Rollins et al *(14)* studied the pile downdrag induced by liquefaction. The stress distribution along the flight auger piles were monitored during the blast liquefaction test. The performance of the piles was monitored prior and after the application of the loads at the top of the piles. Small explosive charges were used to liquefy the soil around the pile. For the first case where there is no load applied to the top of the pile, the location of the neutral plane was within the liquefied layer of soil. It was also found that positive skin friction was induced below the neutral plane within the liquefied layer *(14)*. This was in contrast with some design procedures, which suggested that the location of the neutral plane should be at the bottom of the liquefied layer. Based on the stress distribution along the pile length, the neutral plane was the point along the pile, where the stress started to decrease. It was also found that the unit skin friction along the pile was reduced by 50% after the liquefaction as compared to its original value. This included both of the negative and positive skin friction because of the presence of the neutral plan within the liquefied zone.

Rollins and Hollenbough *(15)* studied the performance of the piles loaded by dead load after the downdrag induced by liquefaction. After applying the dead load on the top of the piles, a blast induced liquefaction was used to settle the ground around the piles. In this study, the soil settlement had not induced any additional negative skin friction because the pile settlement was more than the soil settlement even within the liquefied layer. It was also noted that the stress at the soil-pile interface after the soil liquefaction was similar to what was observed after liquefaction in the non-liquefied zone. However, the shear stress at the soil-pile interface was reduced by 60% as compared to its value before the soil liquefaction within the liquefied zone *(15)*.

Amoroso et al *(16)* reported the performance of a pile subjected to blast-induced downdrag. In this study, the liquefiable sand layer subjected to an increase in the pore water pressure followed by a reconsolidation. Whereas, the non-liquefiable layer soil layer settled as block. During the soil settlement, downward soil side resistance was developed and accumulated from the top of the pile until the neutral plane. The location of the neutral plane was the point along the pile length where the soil settlement is equal to the pile settlement. It was also noted that the positive side resistance in the non-liquefiable soil layer before the sand liquefaction was similar to the negative side resistance in the same layer after the sand liquefaction. However, the side friction within the liquefiable soil layer was reduced by approximately 50 % of its original its value before the sand liquefaction. *(16)* stated that the drag load induced from the top of the pile to the neutral plane was significant. Therefore, a noticeable increase in the toe resistance of the pile was measured. Moreover, the drag load was sufficient to push the pile down to cause an additional settlement of 4% of the pile diameter.

Kevan et al *(17)* studied the pile performance under downdrag induced by liquefaction. In this study, it was observed that the location of the point along the pile length that experienced the maximum stress was the same location where the soil settlement equal to the pile settlement (neutral plane). It was also noted that the soil-pile skin friction within the liquified soil layer was reduced by 78% of its original value. However, the skin friction along the pile length within the non-liquefied soil layer was not affected a lot *(17)*.

Wang and Brandenberg *(18)* utilized a beam on a nonlinear Winkler foundation solution to model pile downdrag. Their solutions showed that the soil settlement and the pile settlement are not equal at the neutral plane. Instead, the pile settlement velocity is equal to the soil settlement velocity at the neutral plane. This contradicted the Fellenius' definition of the neutral plane where the soil settlement and the pile settlement are identical. Wang and Brandenberg *(18)* stressed that the

assumption in Fellenius' unified design method might deviate from actual loading conditions. For example, soil effective stress increases during soil consolidation, thereby resulting in time-varying shaft resistance and neutral plane depth. Furthermore, tip resistance was assumed constant in the Fellenius' definition, while it varies with the pile tip settlement.

Thus, the inconsistent conclusions of the neutral plane should be further explored, which will be investigated in this research using several fully instrumented lab-scale pile tests. A preliminary analysis of a hypothetical pile showed that pile design could be significantly more conservative and costlier when using AASHTO LRFD Bridge Design Specifications. Therefore, there is an immediate need to investigate the fundamental behavior of piles subject to downdrag and propose modifications to the downdrag and drag load calculations of the AASHTO LRFD Bridge Design Specifications, which will be investigated in this research. Although several field monitoring programs in the literature were successfully conducted on piles under downdrag, no single test case history has provided a complete record of pile performance. For example, some case histories lack pile load test data after downdrag, thus they provided no information about pile resistance at the ultimate state. To supplement the existing field test data base, the PI believes it would be desirable to conduct a lab-scale downdrag test on a fully instrumented pile. The tests would provide data on load distribution (a) prior to fill placement, (b) during downdrag after fill placement, and (c) during axial compression test after downdrag.

Last but not least, Kulhawy *(19)* proposed that the unit side friction was given by $f_s = \sigma_z' \, k \, tan\,\delta$ , where $f_s$ is skin friction, $k$ is lateral earth pressure coefficient, $\sigma_z'$ is vertical effective stress, and $\delta$ is interface angle of friction. Kulhawy *(19)* indicates that the coefficient of lateral earth pressure ($k$) is the most important and difficult parameter to determine. $k$ is a function of the original in situ horizontal stress coefficient $k_0$ and the stress changes caused by construction, loading, and downdrag. However, the variation of $k$ along the pile during the construction, downdrag, and loading processes has not been measured, which will be investigated in this study using an innovative $S_3F$ interface sensor. $S_3F$ sensor can measure shear and normal stresses along the soil-pile interface, which will provide the information on the unit side friction and the coefficient of lateral earth pressure ($k$). This investigation will help provide additional insights on the responses at the soil-pile interface during the construction, downdrag, and loading processes.

# 4. METHODOLOGY

This research is to investigate pile downdrag in consolidating ground using fully instrumented lab-scale pile tests. To achieve the main objective of the study, laboratory tests were performed to calibrate innovative $S_3F$ sensors under similar conditions at the pile-soil interface, which was used to measure the drag load and downdrag along the pile length. Eight direct shear tests were performed to measure the shear-displacement relationships at the soil-pile interface subjected to downdrag. Two fully instrumented pile tests were performed to measure the drag load, downdrag, and neutral plane along the pile length. Also, by using finite element method-based software, ABAQUS, a numerical model was developed to provide a realistic estimation of pile downdrag, which will avoid the conservative pile foundation design and reduce the foundation design and construction cost. The procedures adopted to perform the laboratory tests are provided in the following sections.

## 4.1. $S_3F$ Calibration

$S_3F$ sensor was used to measure the negative skin friction, positive skin friction, and the normal stress. However, $S_3F$ sensor has not been used in geotechnical applications. Thus, $S_3F$ sensor was calibrated for different physical conditions (e.g., effect of the loading area, soil particle size, soil saturation condition and temperature).

The Surface Stress Sensitive Film ($S_3F$) technique uses the 3D deformations of an elastic film to determine the applied normal and shear stresses on the sensor *(20)*. $S_3F$ sensor consists of an elastic film surrounded by a stiff plastic boundary as shown in Figure 2. The whole elastic film has an area with a diameter of 25.4 mm. A metal plate floating in the elastic film locates at the center of sensor (Figure 2). The area of the elastic film above the floating metal plate represents the measurement area of the sensor. $S_3F$ sensor was calibrated under similar conditions at the pile-soil interface to exactly measure the normal stress and the skin friction at the pile-soil interface during the downdrag tests. The size of the measurement area above the floating metal plate is 5x5 mm. The effect of the loading area on the sensor readings was investigated. The effect of the soil particle size, soil saturation condition and temperature are being investigated. Initial results are provided in the analysis and finding section. The calibration procedures are provided in the following subsections.

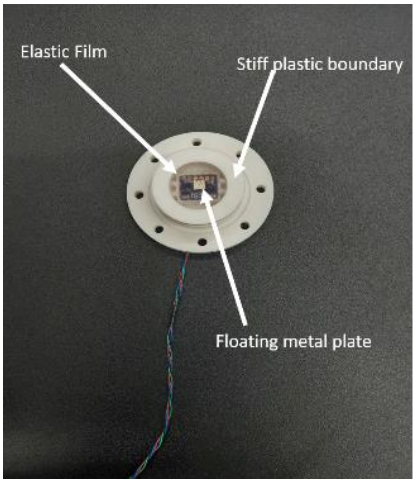


**Figure 2. $S_3F$ sensor details.**

### *4.1.1. Calibration for Low Normal Stress Condition*

The $S_3F$ sensor was subjected to normal pressures ranged from 0 to 35 kPa. Calibration was performed using the following steps: (1) placing the sensor on a horizontally flat surface, (2) connecting the sensor with computer to record the $S_3F$ readings during the tests, (3) applying stresses from 0 to 35 kPa on the sensor using weights (each weight has specific mass and diameter) (Figure 3a), (4) recording the change of the $S_3F$ readings with the change of loading, and (5) creating the calibration curves (applied stress versus recorded $S_3F$ reading). Steps 3 to 5 were repeated five times to investigate the effects of different loading areas on the calibration curves. Five loading areas with diameters of 12, 17.5, 19, 21, and 25 mm were used in the calibration (Figure 3b).

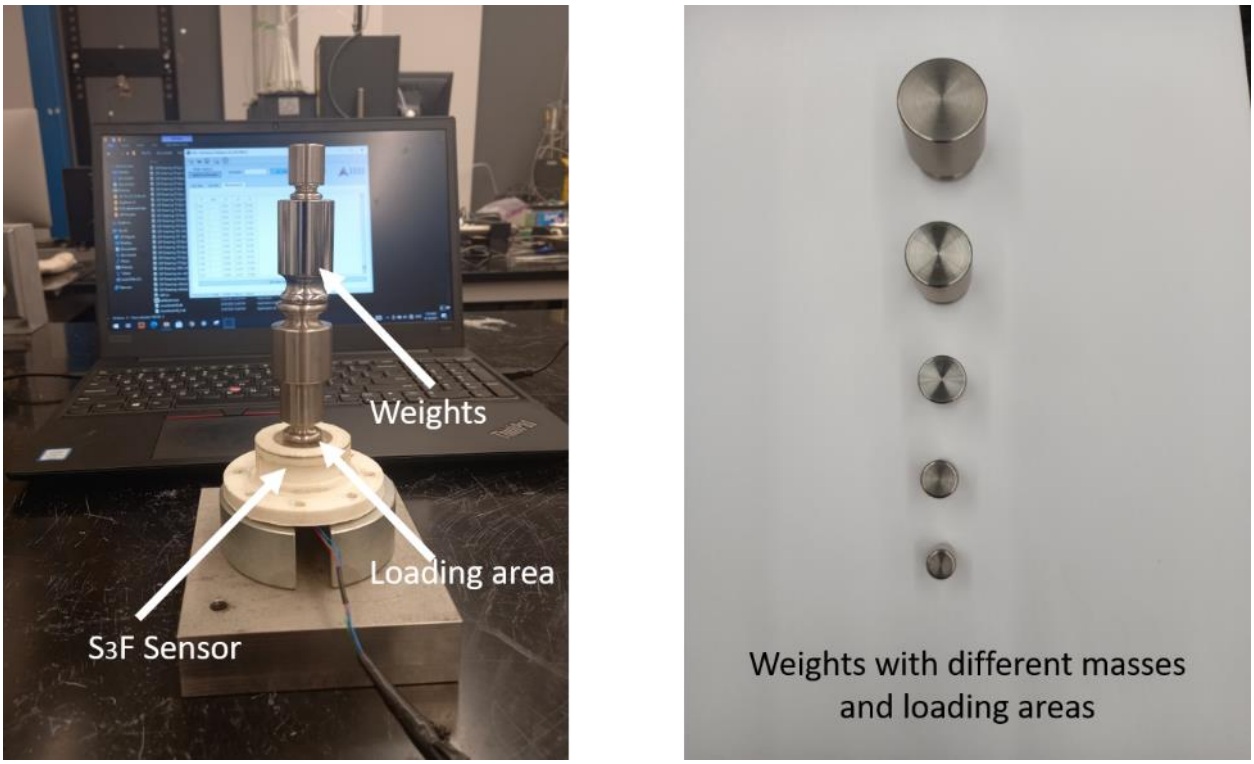


(a) (b)

**Figure 3. Calibration for low normal stress condition: (a) setup, and (b) different weights for loading.**

### *4.1.2. Calibration for High Normal Stress Condition.*

To investigate the $S_3F$ sensor readings under high normal stress condition, $S_3F$ sensor was subjected to different high normal pressures ranging from 35 to 400 kPa. Also, sensor readings under loading/unloading conditions were conducted. This task included two sub-tasks.

The first sub-task was used to measure $S_3F$ sensor readings under increasing applied stress. $S_3F$ sensor was placed in the GeoJac consolidation test device (Figure 4). The GeoJac was used to load the $S_3F$ sensor from 35 to 400 kPa. The same loading area (18 mm in diameter) was used as shown in Figure 4. $S_3F$ sensor readings were recorded by the computer.

The second sub-task was used to assess the $S_3F$ sensor readings under loading/unloading conditions. Same setup as the first sub-task was used. The $S_3F$ sensor received the following load steps in sequence, 400, 100, 50, 150, 300, and 50 kPa. The $S_3F$ sensor readings using calibration relationship of the first sub-task were compared to the GeoJac load cell readings. The accuracy of the $S_3F$ sensor readings was then assessed.

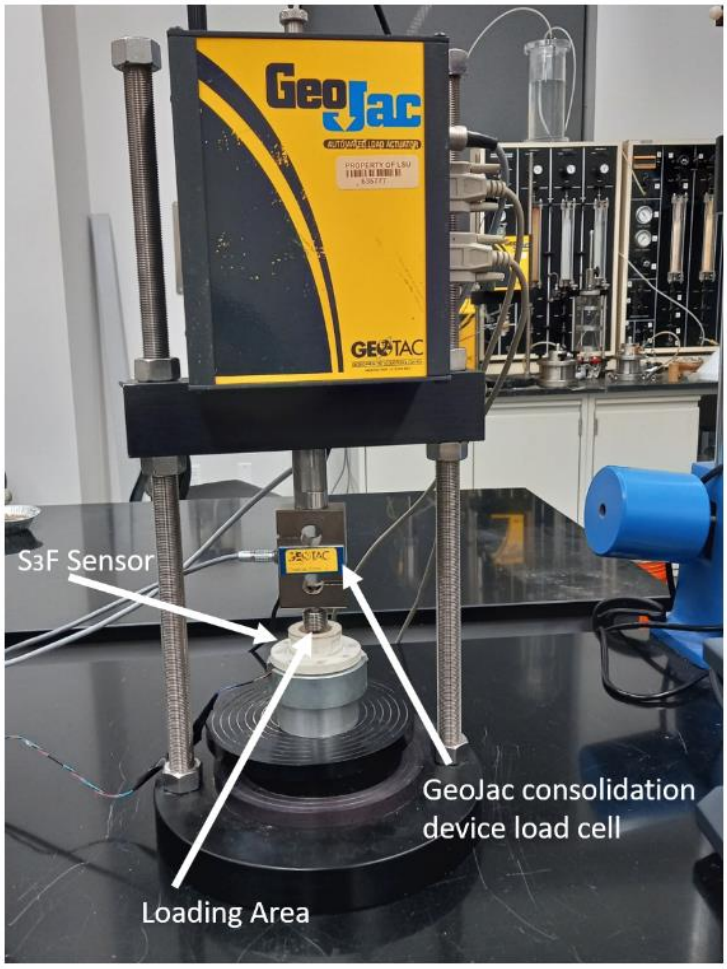


**Figure 4. Setup for $S_3$f sensor calibration under high normal stress condition.**

### *4.1.3. Calibration for Shear Stress*

Shear stress measurement using $S_3F$ sensor was calibrated and subjected to shear stresses ranged from 0 to 60 kPa. The test setup is shown in Figure 5. The sensor was fixed by using plastic clamps on a flat surface. A metal weight with a diameter of 12.5 mm was placed on top of the sensor by using another clamp to apply a constant normal stress on the $S_3F$ elastic film. Then, a tension cord was attached to the metal weight to pull the weight horizontally, which will create shear stress at the metal weight-elastic film interface. A pulley was used to control the direction of the tension cord so that tension cord can apply a horizontal shear force on the $S_3F$ sensor film. Small weights were attached to the other end of the tension cord to apply shear stresses ranging from 0 to 60 kPa. Furthermore, the effect of different loading areas applied on the $S_3F$ sensor film was investigated. The calibration procedure was repeated three times for different loading areas (12.5, 17, 21 mm).

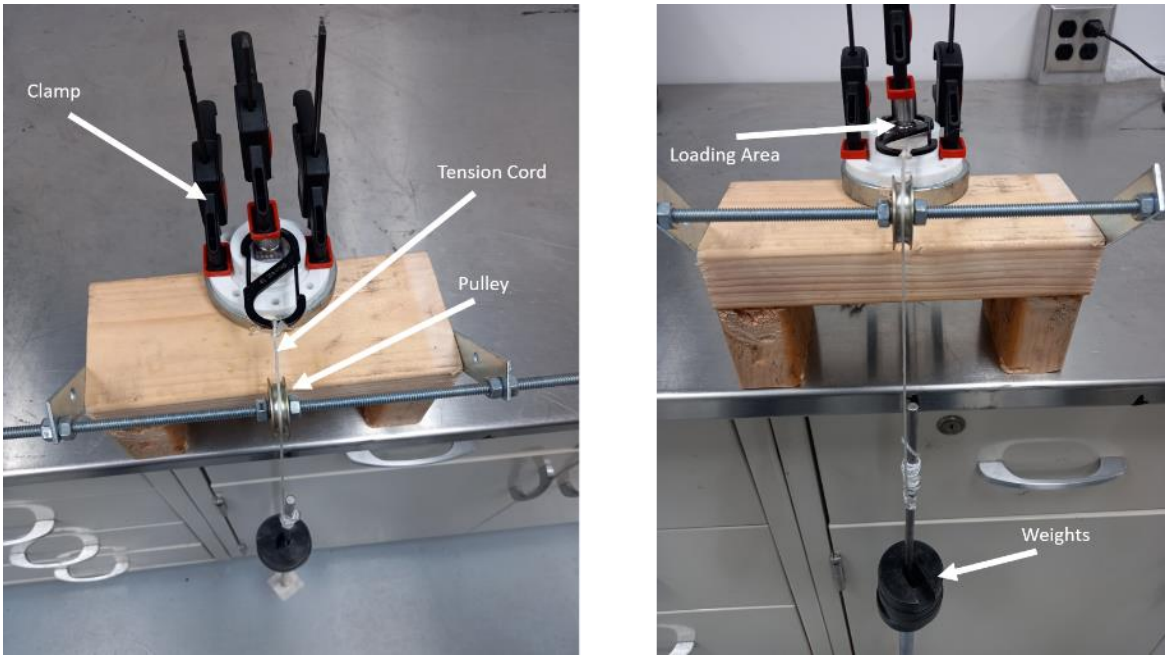


(a) (b)

**Figure 5. $S_3F$ shear calibration setup: (a) top view, and (b) front view.**

## 4.2. Downdrag Tests

The downdrag tests were performed to investigate the drag load, downdrag, and neutral plane along the pile length. Two fully instrumented pile tests were performed. The first pile test was to investigate the floating pile behavior under downdrag (test No. 1). The second test was to investigate the end bearing pile behavior under downdrag (test No. 2). The test setup is shown in Figure 6.

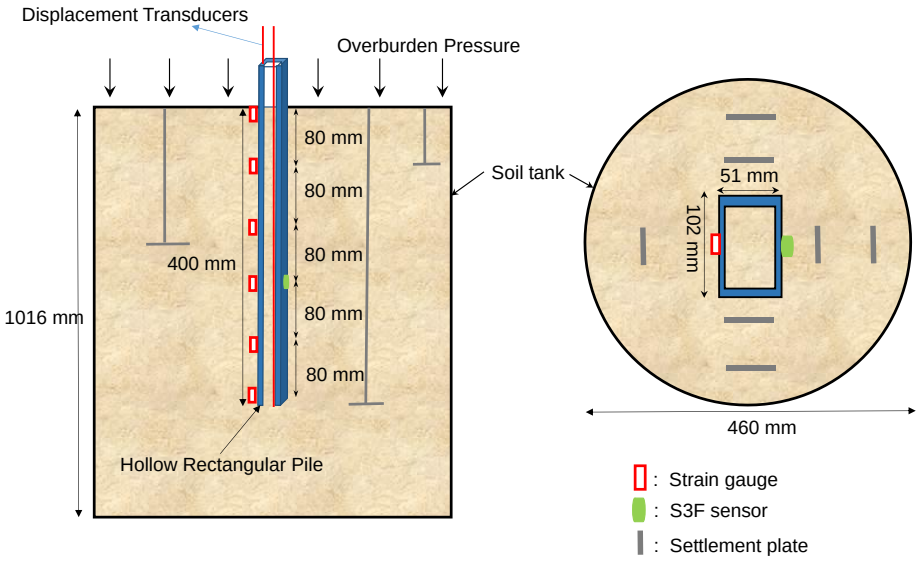


**Figure 6. Pile downdrag test setup.**

A circular soil tank (460 mm in diameter and 1016 mm in height) was used for the tests as shown in Figure 6. The soil tank was filled with water followed by raining Ottawa 50-70 sands into the soil tank. The sand-raining method was to create a loose soil deposit so that the loose sand can experience a large soil settlement during the pile tests (Figure 7a). During the sand preparation a hollow rectangular aluminum pile (51×102×508 mm) was installed inside the soil box (Figure 7b). The tip of the pile was located at the center of the tank at 400 mm below the soil surface. One $S_3F$ sensor was installed at depth of 304 mm to measure the skin friction during the test (Figure 7c). Six strain gauges were installed at the pile surface to measure the stresses along the pile during the test (Figure 7d). The first strain gauge was installed at the bottom of the pile (near the tip), followed by five strain gauges installed along the pile length. The distance between each two consecutive strain gauges was 80 mm. Two displacement transducers were connected to the top and bottom of the pile to measure the pile settlement during the tests. During the test preparation, seven settlement plates were installed inside the soil tank to measure the soil settlement. The tip of the first settlement plate was placed near the pile tip, followed by six settlement plates installed at different depths inside the soil tank (Figure 8a). The distance between each consecutive tips of the settlement plates was 70 mm. After sand raining, a stiff steel loading plate was installed at the soil surface, which was used to apply overburden pressure on the soil by using heavy loading discs (Figure 8b). Seven LVDTs were placed at the top of the settlement plates to measure the settlement of each settlement plate, which was used to plot the soil settlement profile. After sensor instrumentation, uniform overburden pressure was applied at the soil surface to consolidate the soil using loading discs placed on the circular loading plate. Gentle vibration was applied on the outer side of the soil tank to help the soil settling during the test.

For the floating pile downdrag test, the tip of the pile was placed on a very loose sand layer (sand rained inside the tank). On the other hand, a wooden piece was installed inside the soil tank below the tip of the end bearing pile to represent a very stiff layer underneath the tip of the pile (Figure 8c).

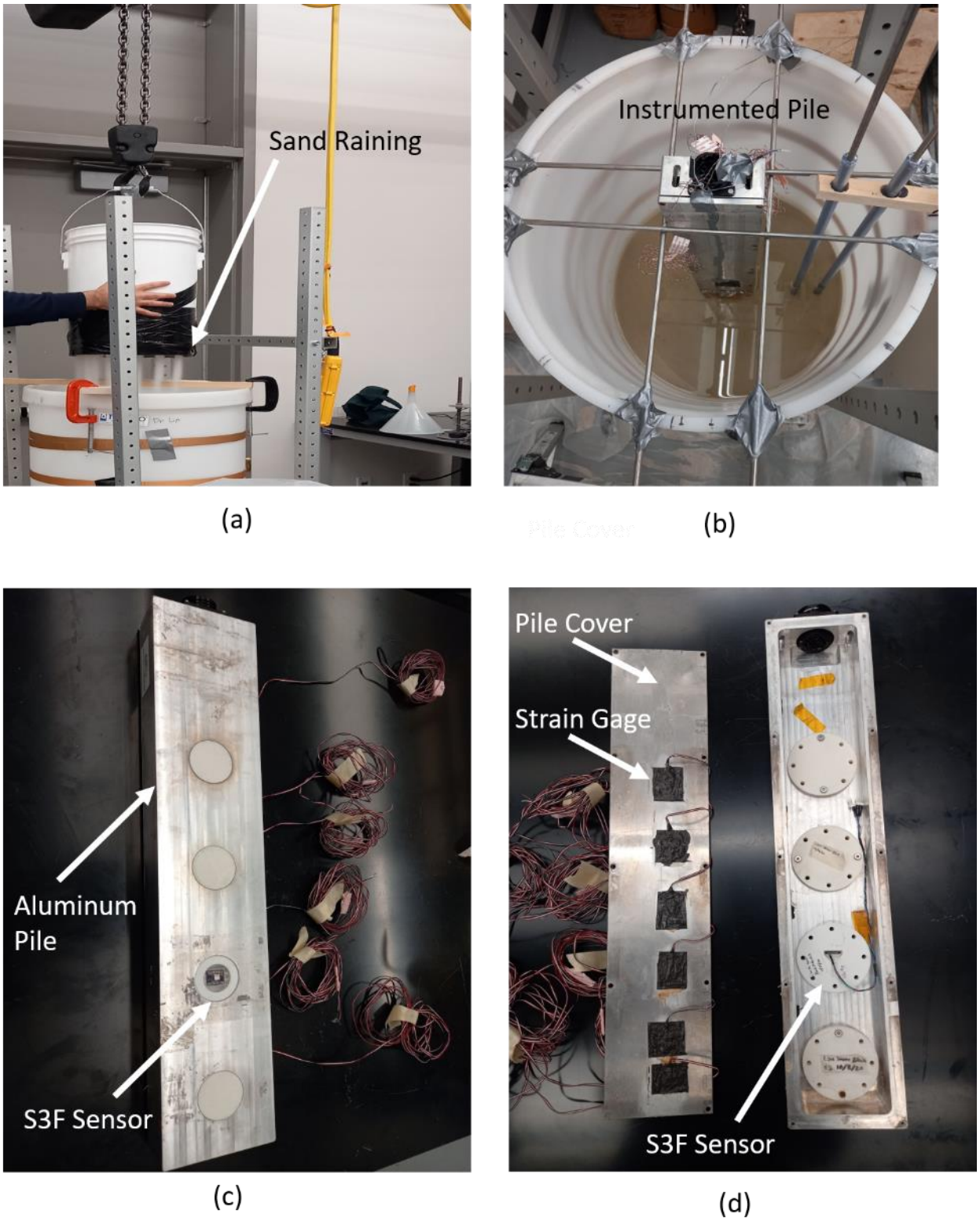


**Figure 7. (a) Sand raining, (b) pile installation in the soil tank, (c) the front of the instrumented pile, and (d) pile instrumentation details.**

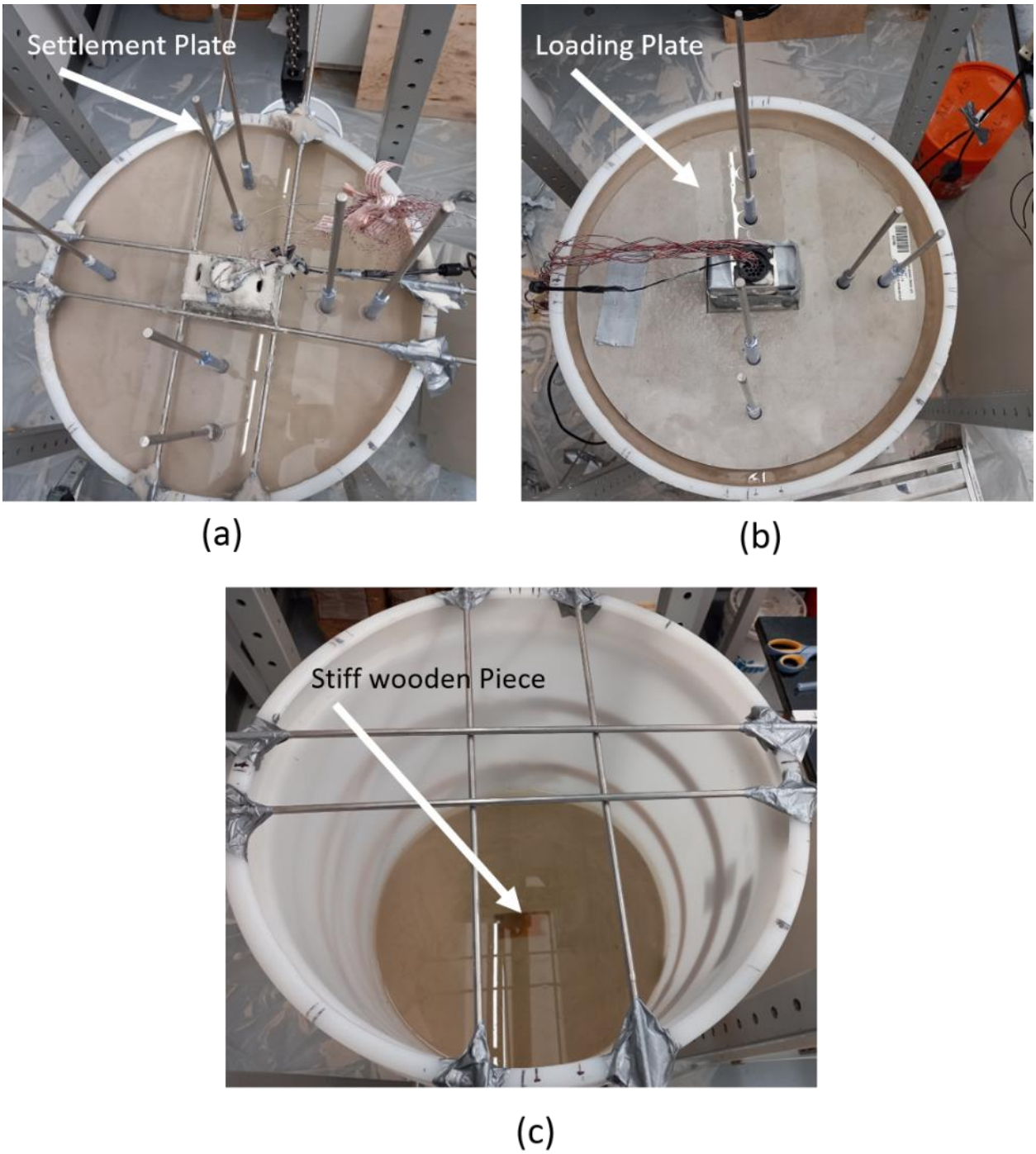


**Figure 8. (a) Settlement plate installment, (b) loading plate at the top of the soil, and (c) stiff wooden piece to support the pile.**

## 4.3. Interface Direct Shear Tests

Direct shear tests can simulate the relative movement between the soil and pile. Direct shear tests were used to measure the interface shear behavior between the soil and pile. As shown in Figure 9, the direct shear test was modified to use the pile material (i.e., aluminum) as the bottom shear box. Ottawa 50-70 sand was prepared in the upper shear box. During the tests, the top shear box was loaded horizontally relative to the bottom shear box to simulate the relative movement between the soil and the pile during pile downdrag. Ottawa 50-70 sand used in the upper soil box was subjected to eight different overburden pressures (e.g., 15, 35, 50, 70, 100, 125, 150, 175 kPa) to investigate the responses at the soil-pile interface under various overburden pressures. The horizontal load cell of the direct shear test device was used to measure the shear stress at the soil-aluminum interface. Horizontal and vertical position transducers were used to measure the relative displacement at the soil-pile interface and the vertical deformation of the soil, respectively.

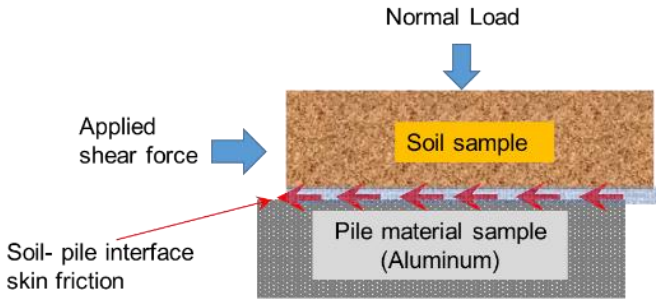


**Figure 9. Direct shear test setup.**

## 4.4. Numerical Modeling and Parametric Analyses

The research team developed a comprehensive numerical model, using the ABAQUS finite element package, to investigate the downdrag and drag load mobilized at the pile-soil surface as well as the overall settlement responses of the pile and surrounding soil with time. Figure 10 shows the finite element mesh configuration used for modelling the pile downdrag laboratory experiments. The FEM mesh was made finer in the zone near the pile where stress concentration is expected, and the elements chosen are C3D8P (eight-node trilinear displacement and pore pressure brick element) for the soil while C3D8 (8-node linear brick element) was used for the pile. The calculation domain adopted was radius (R) = 230 mm and depth (D) = 1016 mm to be consistent with the lab-scale instrumented pile test setup. To simulate the lateral confinement of the soil tank, all the nodes at the bottom/outer radial boundaries were fixed in both displacement and rotation (through the ABAQUS keyword *BOUNDARY).

In the finite element numerical analysis, the sand deposit was modelled as a simple elastic perfectly-plastic Mohr-Coulomb material, for which the two required parameters of friction angle ($\phi'$) and cohesion ($c'$) were provided by the measured Ottawa sand 50/70 properties. Such selected Mohr-Coulomb model should be adequate for the calibration purpose with the laboratory load test data. Moreover, the interfacial behavior and probably the occurrence of pile-soil slip was considered by using suitable master-slave contact elements that are directly available in ABAQUS software. The surface of the pile with greater stiffness was designated as master surface, while the surface of the relatively soft soil was designated as slave surface. The interaction contact between the surface pair is defined by their tangential and normal behavior, using some certain value of the

soil-pile friction coefficient. The ABAQUS FEM simulation intended for measuring the pile downdrag responses was divided into two steps. The first one is a *GEOSTATIC step, in which the effective in-situ stresses pertaining to the laboratory conditions were defined through the *INITIAL CONDITIONS, TYPE = STRESS option. The "CONSOLIDATION" step (including the dissipation of excess pore water pressure), under the lab-scale overburden pressure (see Figure 6a), was established by introducing the keyword *SOIL CONCONSOLIDATION to account for the fully coupled skeleton deformation/fluid diffusion mechanism. This is an ABAQUS built-in feature/command, which requires to break down the transient "CONSOLIDATION" process into sufficiently small sub-steps. To save computational efforts, an automatic time stepping scheme (involving the initial/maximum time step and tolerance on the maximum pore pressure change allowed in one single increment) was used for this simulation step.

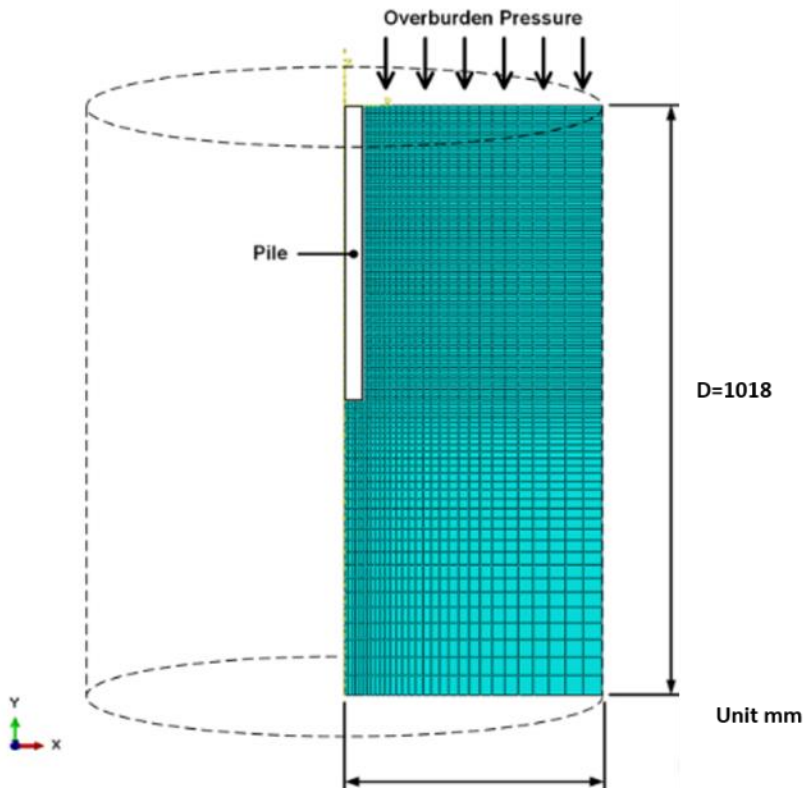


**Figure 10. Finite element meshing for pile downdrag laboratory test.**

# 5. ANALYSIS AND FINDINGS

## 5.1. $S_3F$Calibration Results

### *5.1.1. Results of Low Normal Stress Calibration.*

The normal stress calibration curves between the applied stress and $S_3F$ sensor readings were measured. To assess the effect of the loading areas on calibration curves, five loading areas were investigated. The normal stress calibration curves in Figures 11a, b, c, d, and e represent the calibration curves with loading areas of 12.5, 17, 19.5, 21, and 25 mm diameter, respectively. It is worth noting that the full area of the sensor elastic film has a diameter of 25 mm and it includes the measurement area which locates at the center of the elastic film with a diameter of approximately 7 mm.

Figure 11 indicates that there is a linear relationship between the $S_3F$ normal stress readings and the applied stresses. The calibration curve for the loading area of 12.5 mm (Figure 11a) has a slope of 5.94, while slopes are 5.09, 3.26, 2.44, and 0.17 for loading areas of 17, 19.5, 21, and 25 mm in diameter, respectively. This suggests that the slopes of the calibration curves decreased with increasing loading area. This could be attributed to the stiff boundary that supports the outside of the circular elastic film. The high stiffness of the boundary received higher force when the loading area is large on the circular film, resulting in lower levels of forces at the center of the circular film. The lower forces resulted in lower deflection values at the center of the film. Since the sensor records its reading based on the amount of deflection over the measurement area of the floating metal plate, the rate of change of the $S_3F$ reading with respect to the applied stress decreased as the contact area increased. The maximum grain size of the Ottawa 50/70 sand is 0.3 mm, which is much smaller than the diameter of the measurement area. This demonstrates that the size of the Ottawa 50/70 sand particles will not affect the $S_3F$ reading. Thus, the authors believe that the $S_3F$ can be generally used to measure the normal stress of soil for geotechnical engineering applications. Since the soil particle size is generally less than the diameter of the measurement area, the stresses will be completely transferred from the soil particles to the measurement area. It is recommended to calibrate the sensor by using a contact area that is exactly equal to the measurement area.

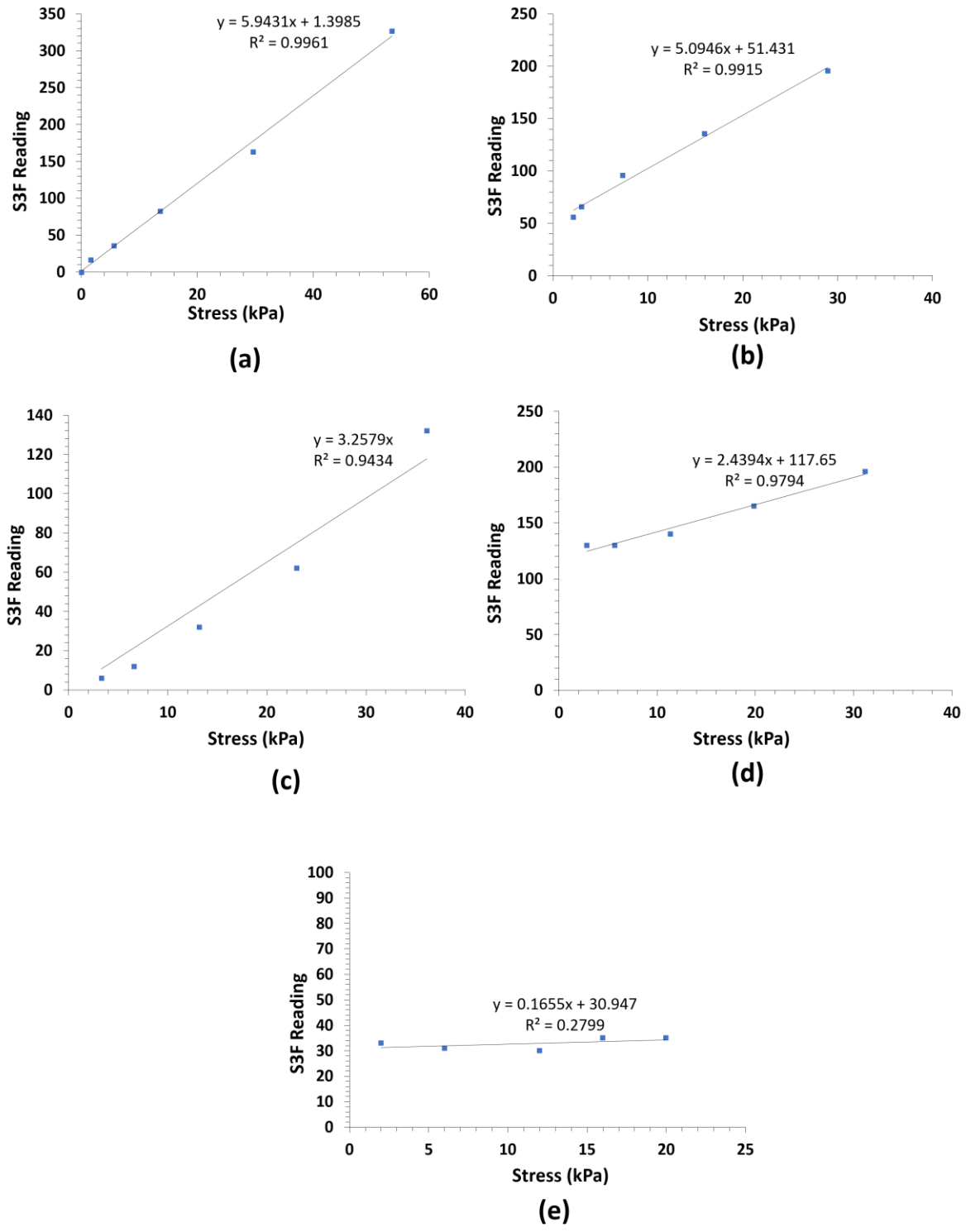


**Figure 11. Normal stress calibration curves with different loading areas: (a) loading area with 12.5 mm diameter, (b) loading area with 17.5 mm diameter, (c) loading area with 19 mm diameter, (d) loading area with 21 mm diameter, and (e) loading area with 25 mm diameter.**

### *5.1.2. Results of High Normal Stress Calibration.*

The normal stresses at the soil-pile interface in the lab-scale downdrag tests were less than 35 kPa. However, the normal stresses in the soil in the field may reach values higher than 35 kPa. Therefore, it is worth investigating the sensor readings at higher pressures than 35 kPa. Also, the response of the $S_3F$ sensor subjected to loading and unloading conditions were investigated. Also, the $S_3F$ normal stress readings and the applied normal stresses were measured as shown in Figure 12a. One loading area with diameter of 18 mm was used during the tests. As shown in Figure 12a, the rate of change of the $S_3F$ readings with respect to the applied normal stress (the slope of the curve) is 4.54. The relationship between the $S_3F$ normal stress readings and the applied stresses is linear. Figure 12b shows the results of the loading/unloading test of the sensor using the same loading area. It shows that the $S_3F$ sensor readings matched the actual applied loading under loading and unloading conditions.

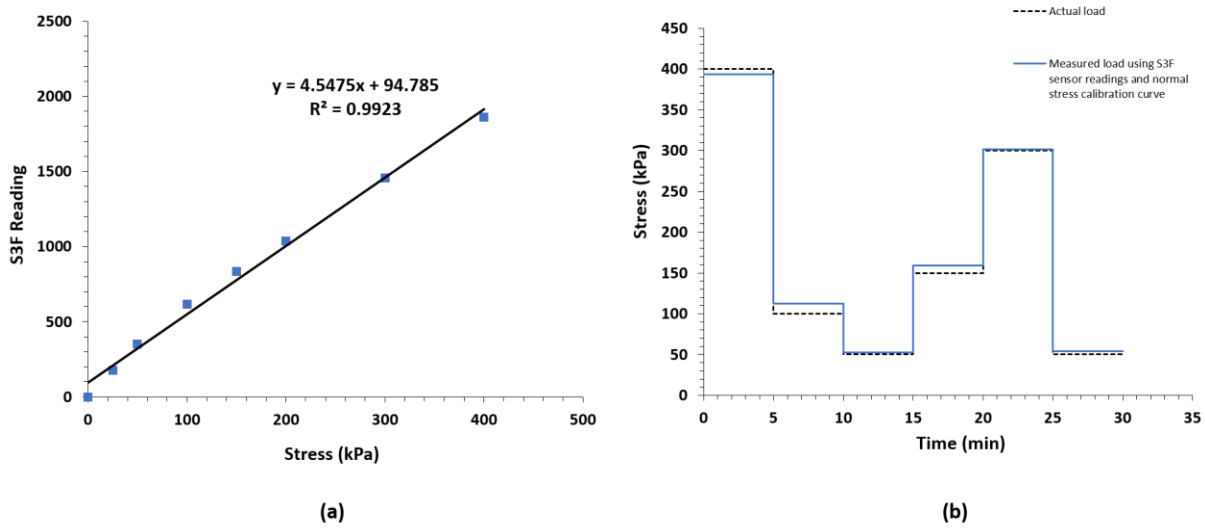


**Figure 12. (a) High normal stress calibration curve with contact area of 18 mm diameter, and (b) S3F readings under loading/unloading conditions compared to the actual load.**

### *5.1.3. Results of Shear Stress Calibration*

The shear stress calibration curves between the applied stresses and $S_3F$ sensor readings were measured. To assess the effect of the loading areas on calibration curves, three loading areas (12.5, 17, and 21 mm in diameter) were investigated. The results of the calibration are shown in Figures 13a, b, and c.

The shear stress calibration curves in Figures 13a, b, and c indicate that there are linear relationships between the $S_3F$ shear readings and the applied shear stresses. The calibration curve for the loading area of 12.5 mm (Figure 13a) has a slope of -10.32, while the slopes are -10.38, and -9.33 for loading areas of 17 and 21 mm in diameter, respectively. This suggests that the slopes of the calibration curves are almost constant regardless of the size of the loading area. This could be attributed to the uniformity of the stress distribution at the interface between the loading area and the elastic film of the sensor. The uniform shear stress distribution at the shear interface resulted in similar levels of deflections and forces at the center of the flexible film (i.e., at the measurement area above the floating metal plate).

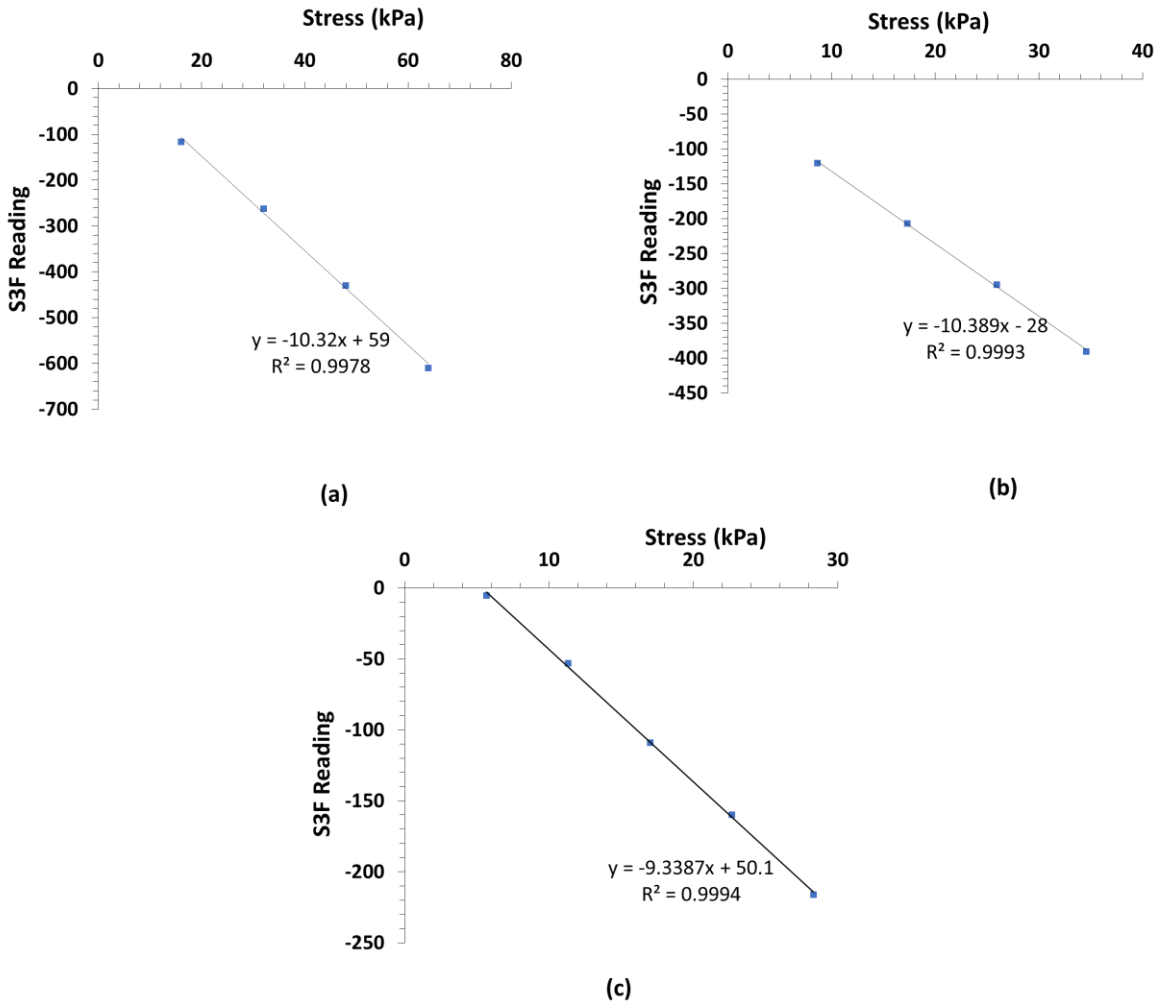


**Figure 13. Shear stress calibration curves with different loading areas: (a) loading area with 12.5 mm diameter, (b) loading area with 17mm diameter, (c) loading area with 21 mm diameter.**

## 5.2. End Bearing Pile Downdrag Test Results

The behavior of an end bearing pile subjected to downdrag was investigated. The sand relative density in this test was around 25%. The pile was an end bearing pile. The readings of the LVDTs at the top of the settlement plates were collected to obtain the soil settlement profile. The strain gauge readings were also collected during the test. Figures 14 and 15 show the soil settlement profiles at different time during the test and the strain gauges readings along the pile during the test, respectively. At the beginning of the test (15 seconds after starting the test), Figure 14 shows that the soil settlement was approximately 5 mm near the tip of the pile and 8 mm at the soil surface. These amounts of settlement could be enough to create a full mobilization of the skin friction. Fellenius *(4, 21)* concluded that the ultimate skin friction could be mobilized by a tiny movement. Figure 15 shows that after 15 seconds of the test, the readings of the second, third, fourth, and fifth strain gauges are approximately the same. This could be attributed to the low level of the effective stress at the beginning of the test. Therefore, the skin frictions at this stage of the test were small, and consequently the strain gauges readings with depth were constant. However, the sixth strain gauge, which locates near the tip of the pile, showed a reading higher than the other

strain gauges. This could be attributed to the high tip resistance. Figure 14 also shows that the settlement of the soil increased with time. However, the slopes of the soil settlement profiles between each two consecutive settlement plates were not the same. This could be attributed to the non-uniformity of the soil settlement, which could happen as a result of the man-made vibration. Figure 15 shows that the readings of each strain gauges increased with time. This is most probably because of the increase in the effective stress with time, which caused the increase in the skin friction and consequently the increase of the stresses in the pile. It was noticed that the water started to pump out from the soil and accumulated above the soil surface during the test. This suggests that there is an increase in the dissipation of the pore water pressure with time. Consequently, there is an increase in the effective stress in the soil with time because the total stress was kept constant during the test. Since Figure 15 showed an increase in the strain gauge readings with depth and the pile was seated on a stiff wood block, the location of the neutral plane was at the tip of the end bearing pile during the test.

The research team will need to perform additional end-bearing pile tests due to the presence of pile bending during the downdrag test. The presence of the pile bending was attributed to non-uniform the man-made vibration on the soil tank. The non-uniform vibration caused a non-uniform settlement at the same soil depth, which created tilting of the loading plate at the top of the soil. As a result, the tilted loading plate caused bending of the pile. The future plan includes attaching mechanical vibrators on the side of the soil tank to create a uniform vibration, which will reduce pile bending during the downdrag test.

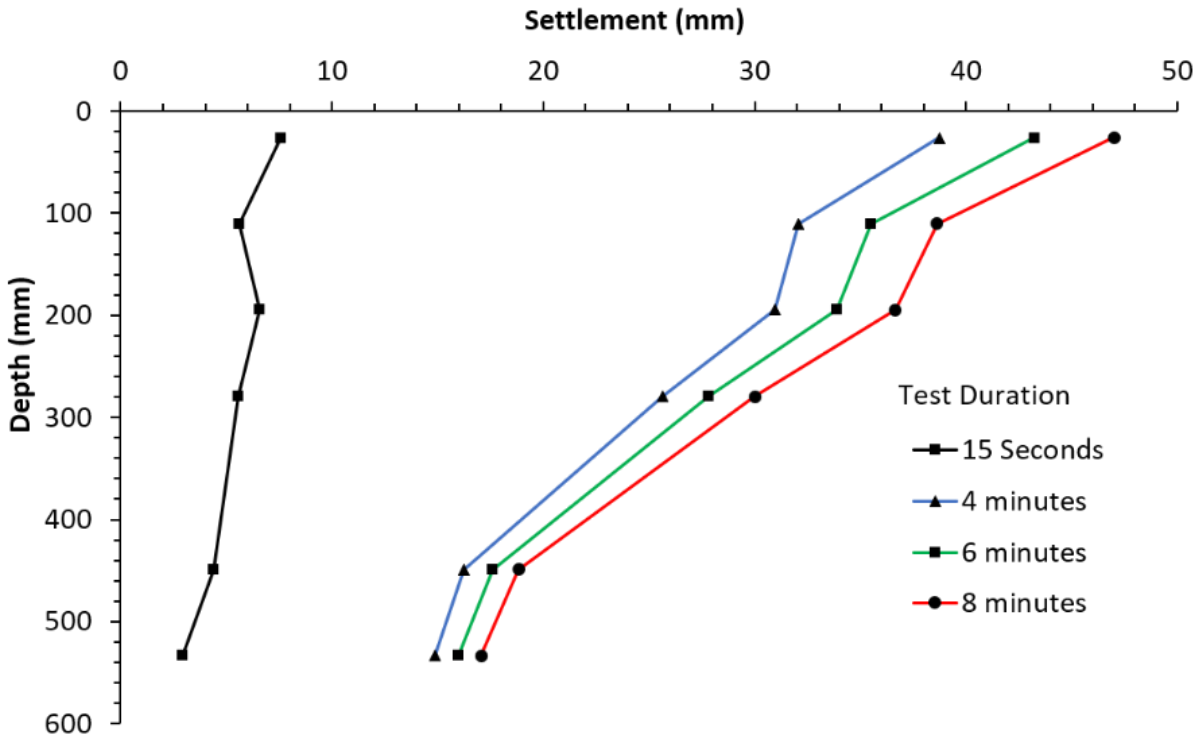


**Figure 14. Soil settlement profiles at different times during the downdrag test.**

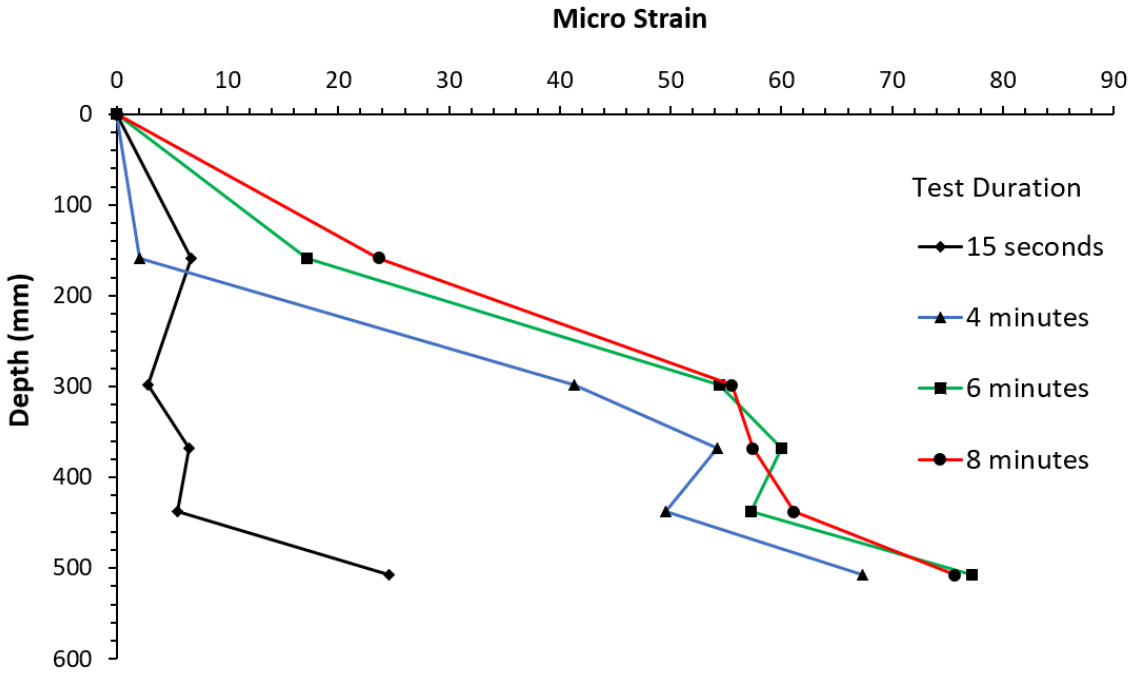


**Figure 15. Strain gauge readings at different time during the downdrag test.**

## 5.3. Floating Pile Downdrag Test Results

The behavior of a floating pile subjected to downdrag was investigated. The soil relative density in this test was around 25%. The pile was a floating pile. The readings of the LVDTs at the top of the settlement plates were collected to obtain the soil settlement profile. The readings of the position transducers were collected during the test to obtain the pile settlement profile. Figure 16 shows the soil settlement and the pile settlement profiles at different time during the test. Figure 16 shows no intersection between the soil and pile settlement profiles during the test, which is contradicted to the literature analysis that pile settlement intersected the soil settlement. It may be due to the absence of the loading on the top of the pile (i.e., dead load). Therefore, the future plans include compression loading on the top of the pile to apply dead load to investigate negative skin friction, drag load, soil and pile settlement profiles, and neutral plane with time.

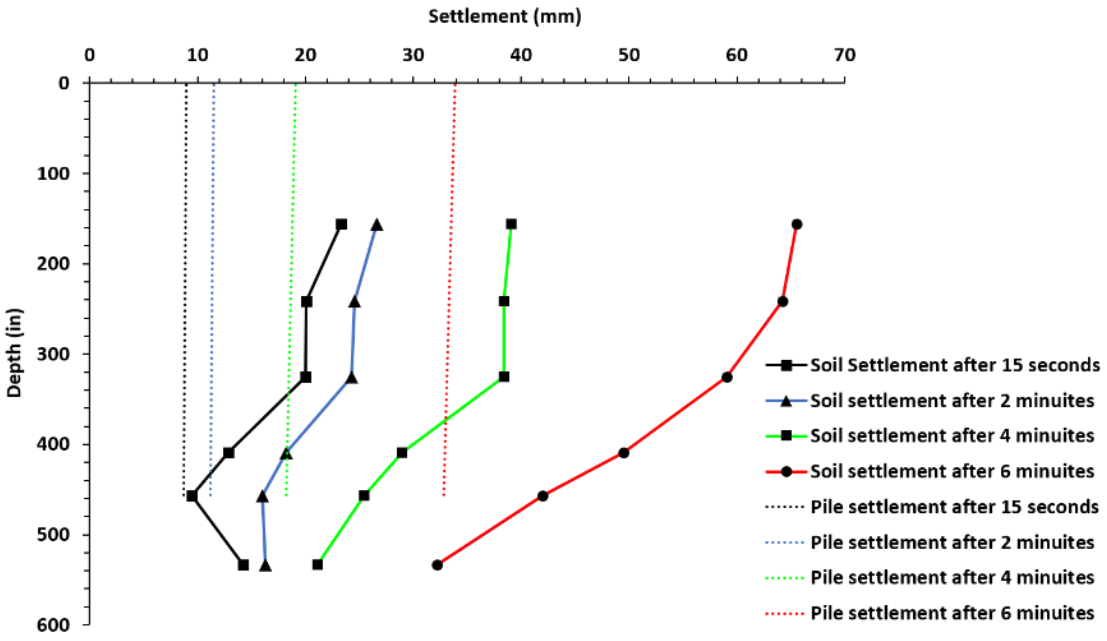


**Figure 16. Soil and pile settlement profiles at different time during floating pile downdrag test the test.**

## 5.4. Results of Interface Direct Shear Tests

The force-displacement relationships at the soil-pile interface were investigated by using the direct shear tests. The readings of the horizontal load cell and the horizontal position transducer of the direct shear test device were recorded during the tests. The readings of the vertical position transducer were also recorded during the tests. Shear stress versus horizontal displacement and vertical displacement versus horizontal displacement were produced from each test as shown in Figures 17 and 18, respectively. Based on the data of each test, Mohr-Coulomb failure envelope with a friction angle of 28.86 was plotted as shown in Figure 19. The friction angle was used for pile behavior analysis and as an input parameter for finite element modeling.

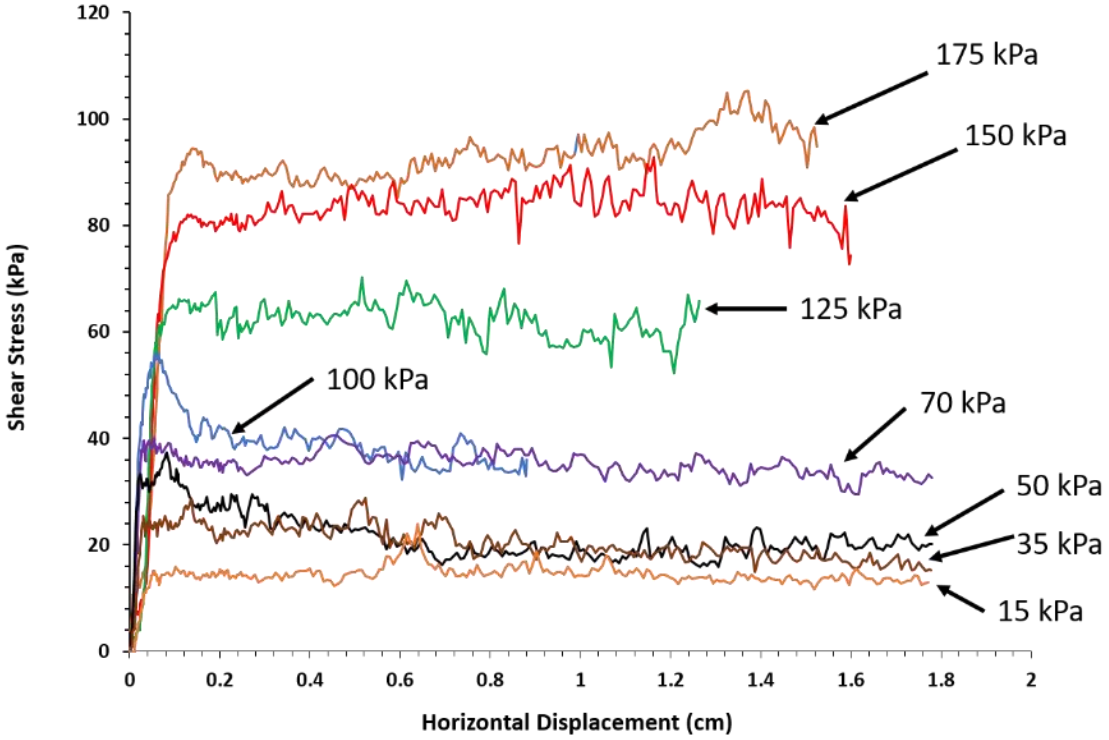


**Figure 17. Shear stress versus horizontal displacement at different overburden pressures during the direct shear tests.**

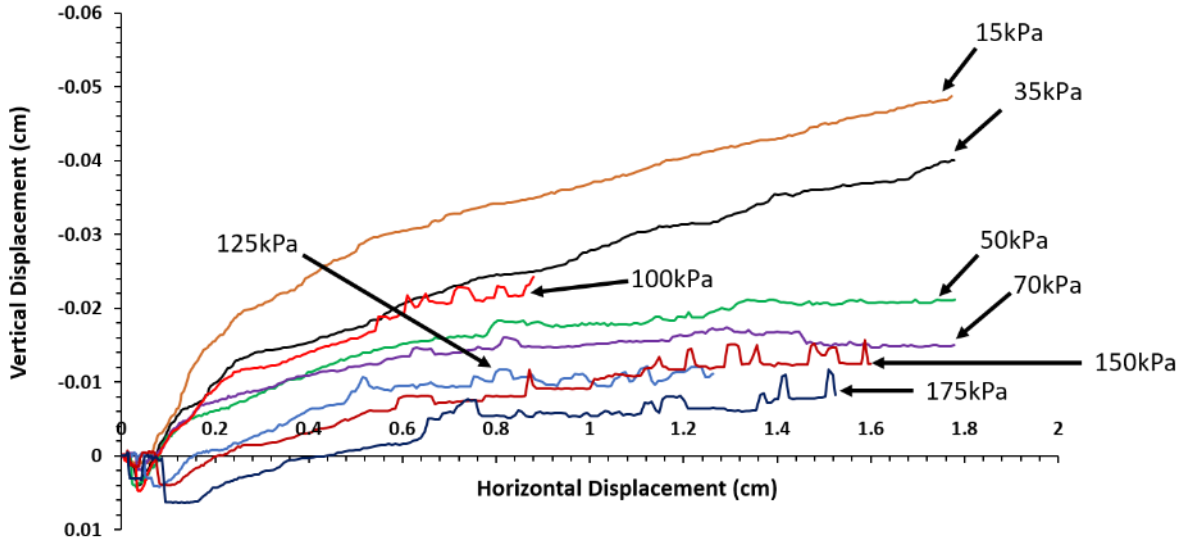


**Figure 18. Vertical displacement versus horizontal displacement at different overburden pressures during the direct shear tests.**

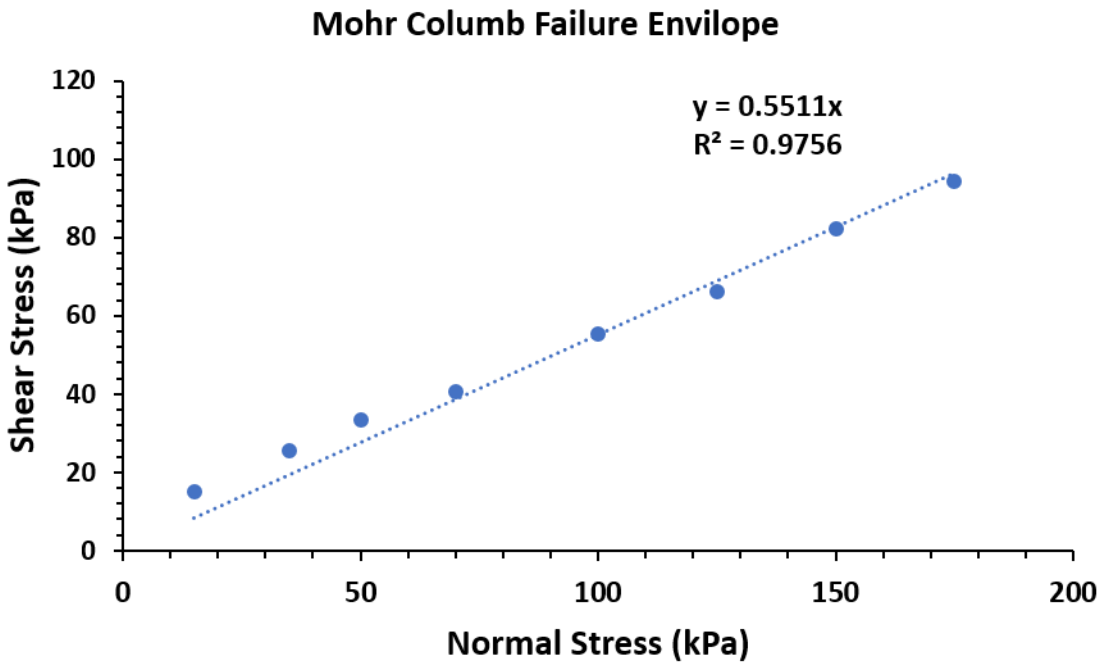


**Figure 19. Mohr-Coulomb failure envelope of direct shear tests at the soil-aluminum interface.**

## 5.5. Numerical Modeling and Parametric Analyses

Developing a numerical model using the ABAQUS finite element package is still ongoing as shown in Figure 20 because the ABAQUS model needs to be calibrated using the experimental test data. Once the experimental tests are completed, the ABAQUS model will be fully calibrated and an extensive parametric analysis will be conducted to cover various combinations of the pile properties and soil conditions in Louisiana. To better simulate the behavior of clayey soil that is frequently encountered in Louisiana, a more realistic and widely accepted elastoplastic model well known as the "modified Cam Clay" will be further considered in the expanded numerical simulations. The five elastic and plastic constitutive parameters featuring the Cam clay model can be obtained from the routine laboratory tests, which indeed are well available from the LADODT geotechnical database and from the published literature. It is expected that the outcomes of such parametric analyses will be able to provide valuable insight into the fundamental mechanism underlying the development/evolution of the pile downdrag and drag load. The numerical modeling, on the other hand, may also serve as a guide to check the potential impacts of the soil box outer boundary on the pile downdrag test results.

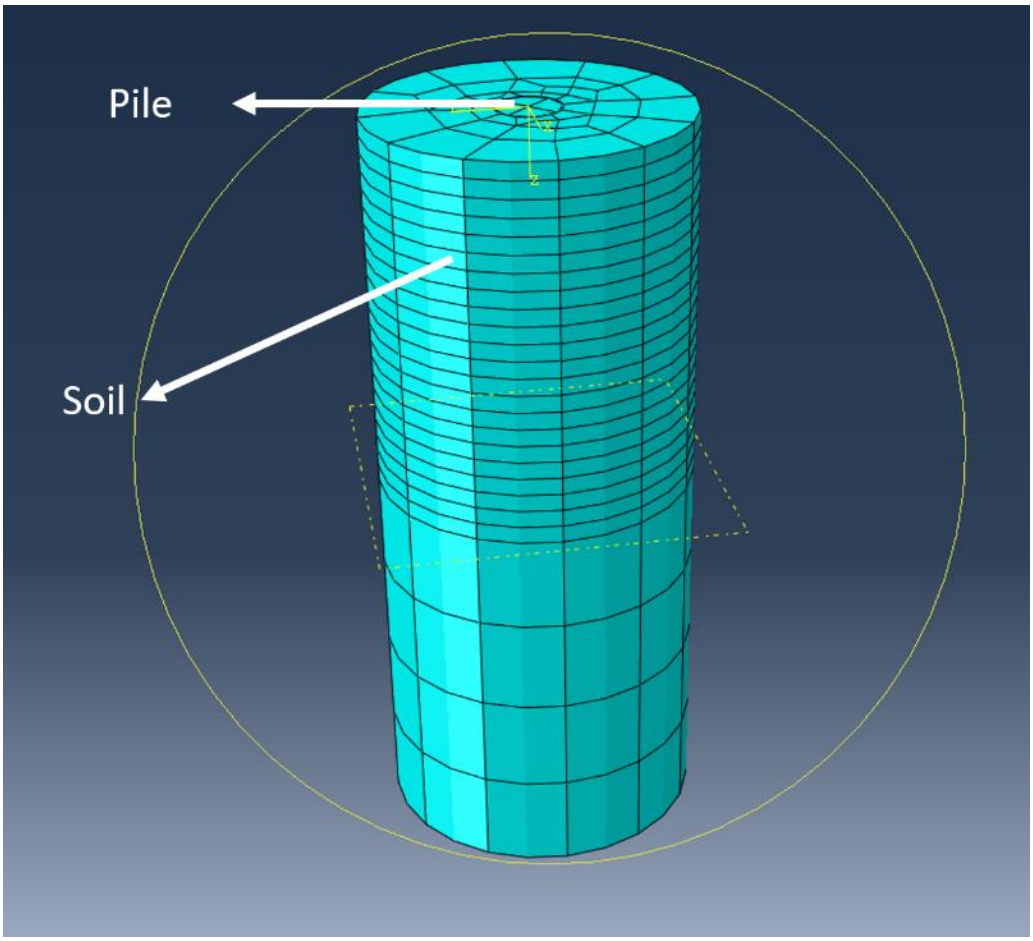


**Figure 20. 3D Finite element meshing for pile downdrag.**

## 6. CONCLUSIONS

The end bearing downdrag test results showed that the drag load increased during the soil settlement despite that the soil-pile relative movement was large enough to create the full mobilization of the skin friction. This suggested that there was a time-varying shaft resistance during the downdrag test. It was also found that the stresses at the bottom of the pile increased with time. Thus, there was a time varying tip resistance. Although the neutral plane location was at the bottom of the end bearing pile, the findings achieved from the end bearing pile test provided valuable insights to investigate the development and the variation of the neutral plane with time and to provide guidance for future floating pile tests. Thus, more floating pile downdrag tests should be performed to confirm the findings and to investigate the development and the variation of the neutral plane with time. It is also recommended to develop a comprehensive numerical model, using ABAQUS finite element package, to investigate the downdrag and drag load mobilized at the pile-soil surface as well as the overall settlement responses of the pile with time. The current study found that literature studies on the variation of the lateral earth pressure coefficient along the pile during downdrag is lacking. Therefore, advanced innovative $S_3F$ sensors will be used to investigate the skin friction development along the pile and the variation of the lateral earth pressure coefficient during pile downdrag. Calibration methods were suggested to calibrate the $S_3F$ sensor under similar conditions at the soil-pile interface. The results showed that

the variation of the $S_3F$ normal readings and the applied normal stresses was linear, and the variation of the $S_3F$ shear readings and the applied shear stresses was also linear. The $S_3F$ showed its ability to respond under loading/unloading conditions. Moreover, the rate of change of the $S_3F$ normal readings with respect to the applied pressure depends on the contact area between the applied load and the $S_3F$ sensor surface. The findings suggested to calibrate the sensor by using a contact area which is equal to the measurement area, and to use the sensor for soils with particle sizes less than 1/10 of the diameter of the measurement area (i.e., 0.5 mm), which includes clay, silt, and fine sand particles.

## REFERENCES


1. Inoue, Y., Tamaoki, K., and Ogai, T. Settlement of building due to pile downdrag. Proc., 9th Int. Conf. on Soil Mechanics and Foundation Engineering, (1977). Tokyo, 561–564.

2. Lam, S.Y., Ng, C.W.W. and Poulos, H.G. "Shielding piles from downdrag in consolidating ground". *Journal of Geotechnical and Geoenvironmental Engineering*, (2013). 139(6), pp.956-968.

3. Tawfiq, K.S. "Laboratory investigation on bitumen coating and polyethylene sheeting for downdrag reduction in piles: a comparative study". *Geotechnical Testing Journal*, (1994). 17(2), pp.171-184.

4. Budge, A.S., Dasenbrock, D.D. and Mattison, D.J.. A Synthesis of Pile Performance Monitoring Projects in Downdrag Environments in Minnesota. In IFCEE 2015, pp. 457-471.

5. Fellenius, B.H. "Results from long-term measurement in piles of drag load and downdrag". *Canadian Geotechnical Journal*, (2006). 43(4), pp.409-430.

6. Chow, S.H. and Wong, K.S. "Model pile pull-out tests using polyethylene sheets to reduce downdrag on cast in situ piles". Geotechnical Testing Journal, (2004). 27(3), pp.230-238.

7. Walker, L.K., & Darvall, P.L. Dragdown on coated and uncoated piles : Conference. Session. 7F, 3R. PROC. EIGHTH INT. CONF. ON SOIL MECH. FOUND. ENGNG, MOSCOW, 1973, V2.1, P257–262.

8. Tawfiq, K.S. "Laboratory investigation on bitumen coating and polyethylene sheeting for downdrag reduction in piles: a comparative study". *Geotechnical Testing Journal*, (1994). 17(2), pp.171-184.

9. Fellenius B.H. Observations and analysis of wide piled foundations. *Canadian Geotechnical Journal*, 2019. 56(3): 378–397.

10. Fellenius, B.H.. Unified design of piled foundations with emphasis on settlement analysis. Honoring George G. Goble — Current Practice and Future Trends in Deep Foundations. Geo-Institute Geo TRANS Conference, Los Angeles, July 27-30, 2004, Edited by J.A. DiMaggio and M.H. Hussein. ASCE Geotechnical Special Publication, GSP 125, pp. 253 - 275.

11. Siegel, T.C., GE, D., Brown, D. and Axtell, P.J. "Alternative design approach for drag load and downdrag of deep foundations within the LRFD framework". *Deep Foundation Institute*, (2013).

12. Sears, Brian Keith "Pile Downdrag During Construction of Two Bridge Abutments". *Theses and Dissertations*. (2008).

13. Okabe, T. Large negative friction and friction-free pile methods, Proc., 9th Int. Conf. Soil Mech. Found. Eng., (1977). Vol.1, pp.679-682.

14. Rollins KM, Strand SR, Hollenbaugh JE. Liquefaction induced downdrag and dragload from full-scale tests. In: Developments in earthquake geotechnics. Springer, (2018). pp 89–109.

15. Rollins, K. M., & Hollenbaugh, J. E. Liquefaction Induced Negative Skin Friction from Blast-Induced Liquefaction Tests with Auger-Cast Piles. Procs., 6th International Conference on Earthquake Geotechnical Engineering (p. 8). Christchurch, NZ: New Zealand Geotechnical Society, (2015).

16. Amoroso, S., Milana, G., Rollins, K.M., Comina, C. Minarelli, L. Manuelo, M.R., Monaco, P. et al. The First Italian Blast-Induced Liquefaction Test (Mirabello, Emilia-Romagna, Italy):Description of Experimental and preliminary Results. Annals of Geophysics, (2017). Vol. 60, No. 5, 19 p.

17. Kevan, Luke Ian,."Full-Scale Testing of Blast-Induced Liquefaction Downdrag on Driven Piles in Sand". *Theses and Dissertations*, (2019). .

18. Wang, R. and Brandenberg, S.J. "Beam on nonlinear Winkler foundation and modified neutral plane solution for calculating downdrag settlement". *Journal of geotechnical and geoenvironmental engineering*, (2013). 139(9), pp.1433-1442

19. Kulhawy, F. H. "Drilled shaft foundations." Foundation engineering handbook, 2nd Ed., H. Y. Fang, ed., Van Nostrand-Reinhold, New York,(1991).

20. Fonov, S.D., Jones, E.G., Crafton, J.W., Goss, L.P., Using surface stress sensitive films for pressure and friction measurements in mini-and micro-channels. In: 22nd International Congress on Instrumentation in Aerospace Simulation Facilities, 2007 (ICIASF 2007), June 2007, pp. 1-7. IEEE.

21. Fellenius, B.H. Basics of foundation deign, electronic edition, (2021).